THE JOURNAL OF PHYSICAL CHEMISTRY B

Article

Cite This: J. Phys. Chem. B 2018, 122, 10377−10383

pubs.acs.org/JPCB

Charge-Controlled Surface Properties of Native and Fluorophore-Labeled Bovine Serum Albumin at the Air−Water Interface

Manuela E. Richert,[†] Natalia García Rey,[†,‡] and Björn Braunschweig*[,†,‡]

[†]Institute of Physical Chemistry, Westfälische Wilhelms-Universität Münster, Corrensstraße 28/30, 48149 Münster, Germany

[‡]Center for Soft Nanoscience, Westfälische Wilhelms-Universität Münster, Busso-Peus-Straße 10, 48149 Münster, Germany

Supporting Information

ABSTRACT: Proteins at interfaces are important for protein formulations and in soft materials such as foam. Here, interfacial stability and physicochemical properties are key elements, which drive macroscopic foam properties through structure−property relations. Native and fluorescein isothiocyanate-labeled bovine serum albumin (BSA) were used to modify air−water interfaces as a function of pH. Characterizations were performed with tensiometry and sum-frequency generation (SFG). SFG spectra of O−H stretching vibrations reveal a phase reversal and a pronounced minimum in O−H intensity at pH values of 5.3 and 4.7 for native and labeled BSA, respectively. This minimum is attributed to the interfacial isoelectric point (IEP) and is accompanied by a minimum in surface tension and negligible ζ-potentials in the bulk. Interfacial proteins at pH values close to the IEP can promote macroscopic foam stability and are predominately located in the lamellae between individual gas bubbles as evidenced by confocal fluorescence microscopy. Different from the classical stabilization mechanisms, for example, via the electrostatic disjoining pressure, we propose that the presence of more close-packed BSA, because of negligible net charges, inside the foam lamellae is more effective in reducing foam drainage as compared to a situation with strong repulsive electrostatic interactions.

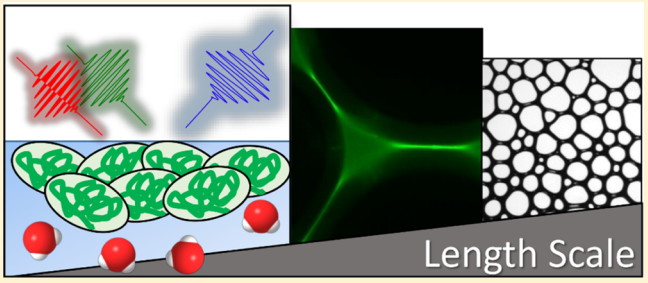

INTRODUCTION

Proteins at interfaces are of great importance in many fields of research such as medicine and pharmacy, for example, for antibody formulations.[1,2] In fact, many diseases such as Alzheimer and Parkinson have been linked to the formation of amyloids—protein aggregates which form fibrils.[3]

In soft matter materials, proteins act as stabilizers, for instance, in foam and emulsions that are relevant for dairy products.[4,5] In case of the latter, protein aggregation in aqueous foams is highly desirable and can be used to make foams more stable, with different viscoelastic properties and microstructures.[6−16] However, for pharmaceutical and antibody formulations, protein adsorption as well as aggregation[17] of proteins in the bulk and at interfaces is also of great interest but with exactly the opposite goal. In fact, in this case foam formation as well as aggregate formation in the bulk and at the unavoidable interfaces, for example, the gas−liquid interface between bulk solution and the headspace of a vial needs to be prevented.[2,18]

Interactions of proteins at interfaces can be characterized by the protein surfaces that have hydrophobic patches because of nonpolar amino acids such as Gly or Leu which are one cause of the amphiphilic character and surface activity of a great number of proteins.[11,19] Amino acid residues like Glu, Asp, or Arg cause pH-dependent charging. The isoelectric point (IEP), at which the net charge of the protein is zero, is thus an important parameter from which the colloidal stability of protein solutions is predicted. Repulsive electrostatic interactions are minimized at pH values close to the bulk IEP. In this case, proteins in solutions with a pH close to the bulk IEP tend to form multilayers at air−water interfaces.[6,7,13,14] In addition, adsorption layers at a solution pH close to the IEP, show high elasticity E' and low viscosity E'' in surface dilatational rheology, whereas at pH values much smaller or higher than the bulk IEP monolayers with strong repulsive electrostatic interactions but small E' are formed.[6,20−22] The classical view within the Derjaguin−Landau−Verwey−Overbeek (DLVO)[23−25] theory predicts for strong repulsive electrostatic interactions, a high electrostatic disjoining pressure[24] in foam films and one would expect—within this classical picture—more stable macroscopic foams at a pH value where the interfaces are highly charged. Indeed Gochev et al.[26] report such behavior for protein solutions and show the formation of Newton black films at a pH around the proteins' IEP, but they also observe aggregates in their foam films. The low electrostatic disjoining pressure around the IEP leads to instable foam films, and however, this is valid at low protein concentration, whereas increase of the protein concentration leads to increase of the film stability.[27] Indeed, at high protein concentration, most stable macroscopic foams from bovine

Received: July 6, 2018
Revised: October 15, 2018
Published: October 19, 2018

DOI: 10.1021/acs.jpcb.8b06481
J. Phys. Chem. B 2018, 122, 10377−10383

serum albumin (BSA)[7] and β-lactoglobulin (BLG)[6] have been reported at a pH close to the proteins' bulk IEP. Besides foam stability, also the foam structure (see below) and rheology[6,28] change around the IEP quite substantially.

So far, the origin of this anomalous stabilization of foams has not been fully resolved, but there is mounting evidence that protein aggregates at the interface play a dominant role in foam stabilization. Rullier et al.[8,9] show in their study on foam films and foams from solutions that contained BLG aggregates and monomers that the highest foam stability is due to synergistic effects between aggregates and monomeric proteins.

Although the origin of foam stabilization by proteins and their exact position within foam remains unresolved so far, the situation for Pickering foams with inorganic particles and organic particles such as surfactant precipitates or vesicles is much clearer.[29−31] Carl et al.[30] studied foams from solutions with silica nanoparticles that have been made more hydrophobic with short-chain amines and reported particle accumulation inside the plateau borders. The silica particles blocked the plateau borders which were proposed to slow down foam drainage and thus to prevent or hinder an important foam destabilization mechanism. Similar effects have also been reported for mixed solutions of 12-hydroxy stearic acid and ethanol amines by Fameau et al.[31] The molecules in these mixtures self-assemble into long tubular vesicles which do not reduce drainage but can efficiently inhibit film breaking and thus give rise to ultrastable foams with half lifetimes of many months.

As proteins act on comparable length scales, it can be hypothesized that they show a behavior similar to the abovementioned particle-stabilized systems. Indeed, such a behavior was shown for thermally gelated whey proteins: by producing foam from solutions with protein gels, the foams were shown to be more stable, and the authors argue that aggregates between the foam bubbles, for example, within the plateau borders reduce foam drainage and are thus a cause for the observed increase in foam stability.[32,33]

So far, for native proteins such as BSA or BLG, investigations regarding the location of aggregates only took place for a single lamella or a single air bubble.[9,14,26,34] To the best of our knowledge, the location of proteins and their possible aggregates directly in the foam has not been studied in detail. For that reason, we present in our study results on structure−property relations within protein stabilized foams. Using a unique combination of experimental methods, we gain information from the molecular to the macroscopic length scale. For that, we have applied vibrational sum-frequency generation (SFG) and tensiometry to interrogate the interfacial molecular structure and its (net)charging state, whereas fluorescence microscopy and foam analysis provide information on larger length scales. In addition, we compare native with fluorescein isothiocyanate-(FITC) labeled BSA proteins which we use to localize the proteins with fluorescence microscopy. This comparison is necessary because previous works have shown that differences in surface properties between native and labeled proteins can exist.[34]

EXPERIMENTAL SECTION

Sample Preparation. Native BSA was purchased as lyophilized powder from Sigma-Aldrich (A7030) with a free fatty acid content of ≤0.02% and was used as received. The albumin-FITC conjugate (FITC-labeled BSA) was also purchased from Sigma-Aldrich (A9771). FITC binding to BSA changes the molecular weight from 66.4 to 71.1 kDa, and 20% of the lysine amino residues in BSA were labeled, both calculated according to the information of the supplier.

If not stated otherwise, sample solutions with 50 μM (labeled or native) BSA were prepared by dissolving the proteins in ultrapure water (18.2 MΩ cm; total organic carbon < 5 ppb). This leads to a pH of the solution of ∼7 for native and ∼8.6 for FITC-labeled BSA. Subsequent to the dilution of the proteins, the solutions' pH was adjusted by adding small aliquots of 0.1 or 1 M HCl or NaOH aqueous solutions. Care was taken to avoid bleaching of the fluorescent label by the room lights and by too acidic pH values. To ensure cleanliness of the samples, the used glassware was soaked in a mixture of concentrated sulfuric acid (analytical grade) and NOCHROMIX for at least 12 h. Subsequently, the glassware was extensive rinsed with ultrapure water. All experiments were performed at room temperature 297 K.

Sum-Frequency Generation. SFG spectra were recorded using ssp polarizations (s: SFG, s: visible, and p: IR beams) with the experimental setup reported in the Supporting Information. For measurements around the protein's IEP, the pulse energies of the broadband IR and the visible beam were reduced to 10 and 11 μJ, respectively. This was necessary to avoid laser-induced changes, for example, desorption, which were observed otherwise. In our experiments with the FITC-labeled proteins, we did also observe multiphoton fluorescence which was caused by the visible beam. The fluorescence photons were blocked with a longpass filter (FF01-593/LP-25, Semrock) which was inserted into the SFG beam path. Full SFG spectra were recorded for C−H and O−H stretching vibrations (2800−3800 cm^{-1}) by scanning the IR frequency in five steps. Depending on the signal strength, the acquisition time per IR wavelength was between 1 and 6 min.

ζ-Potential. ζ-potential measurements were done with Zetasizer Nano ZS (Malvern Instruments). Each pH value was measured at least 3 times, and the mean value was calculated.

Tensiometry. The surface tension γ of a protein solution was measured in a pendant drop tensiometer (Krüss DSA 100) via drop shape analysis using the Young−Laplace equation.

Confocal Microscopy. Scanning confocal fluorescence microscopy of foamed solutions with FITC-labeled BSA was done with a Leica SP8. For excitation, we have used a 65 mW argon laser at a wavelength of 496 nm, and the fluorescence emission was recorded at a wavelength of 520 nm.

Foam Stability. Investigations on the foam stability were done with a Krüss dynamic foam analyzer (DFA 100) and the corresponding foam structure analysis module. The device is equipped with an optical sensor for liquid and foam height detections. Foams were produced in a glass column with a diameter of 4 cm by a 0.3 L min^{-1} gas flow of ambient air for 30 s. Here, we used a porous glass frit with a pore size of 16−40 μm and a sample volume of 60 mL. Pictures of the two-dimensional foam structure near the column wall were taken with the help of a prism that was attached to the column.

RESULTS AND DISCUSSION

A precursor for interface adsorption of proteins is their bulk state and in particular their bulk charging state, which can be studied by ζ-potential measurements. In Figure 1a, the ζ-potentials of native and FITC-labeled BSA proteins are shown as a function of bulk pH. Changing the pH leads to substantial changes in the ζ-potential for both proteins. A close inspection of Figure 1a shows that the bulk IEP of native BSA is at a pH

DOI: 10.1021/acs.jpcb.8b06481
J. Phys. Chem. B 2018, 122, 10377−10383

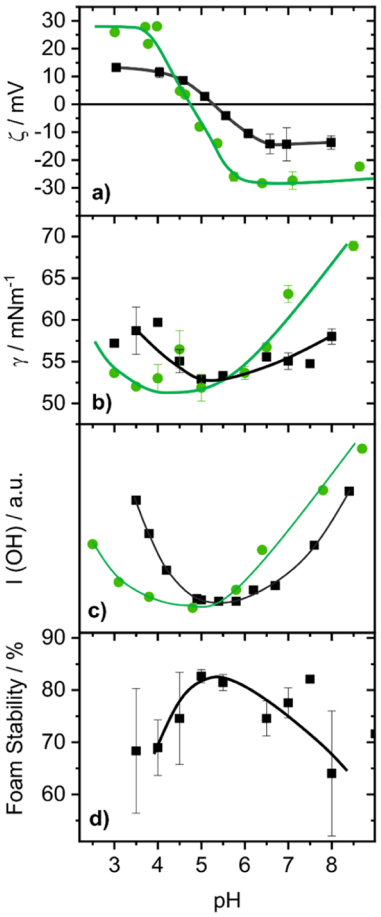

Figure 1. Effects of the bulk pH (rounded to 0.5 steps) for 50 μM BSA solutions on (a) the ζ-potential, (b) the surface tension γ after 30 min equilibration time, and (c) the averaged SFG intensity from the O−H stretching bands between 3150 and 3650 cm^{-1} (SFG spectra are shown in Figure 2). (d) Presents the foam stability (here defined as loss in foam height) after 30 min aging time in percent of the maximal foam height directly after foam formation (0 min). The results for native BSA are represented in black squares, whereas those for FITC-labeled BSA are represented by filled green circles. Solid lines guide the eye.

of ∼5.3, while the IEP of FITC-labeled BSA is shifted to a pH of 4.7. In addition, the absolute values of the maximum ζ-potentials which are established at more acidic and alkaline conditions relative to the protein's IEP are ∼13 and ∼28 mV for native and FITC-labeled BSA, respectively. The results for native BSA are in perfect agreement with previous work,[7] whereas the changes in ζ-potential of the labeled BSA compared to the native protein result from the blocked ε-amino group of Lys residues and by the additional carboxylic acid group of the fluorophore.[34−36]

In order to investigate the charging state of BSA adsorbate layers at the air−water interface, we applied vibrational SFG, which is a second-order nonlinear optical method, that is, inherently interface specific for centrosymmetric materials such as liquids and gases. For SFG, we combine a tunable broadband IR with a narrowband visible pulse at the interface, where the sum frequency (SF) ω_{SF} is generated as a sum of the impinging light waves with frequencies ω_{IR} and ω_{vis}. The intensity of the resulting SF signal is proportional to nonresonant and resonant contributions to the second-order susceptibility $\chi^{(2)}$ and to the third-order susceptibility $\chi^{(3)}$, that is, directly dependent on the surface potential ϕ_0[37−42]

$$I(\omega_{SF}) \propto \left|\chi^{(2)} + \frac{\kappa}{\kappa + i\Delta k_z}\chi^{(3)}\phi_0\right|^2 \quad (1)$$

with

$$\chi^{(2)} = \chi^{(2)}_{NR} + \sum_k \frac{A_k\, e^{i\theta}}{\omega_k - \omega_{IR} + i\Gamma_k} \quad (2)$$

and

$$A_k = N\int f(\Omega)\beta_k(\Omega)d\Omega \quad (3)$$

In eq 1, κ, Δk_z are the inverse of the Debye length and the phase mismatch of the impinging light waves. The surface potential ϕ_0 is caused by the net charge of the adsorption layer and the resulting static electrostatic field. Note that the prefactor to the third-order contribution simplifies at high ionic strengths to one. In eq 2, A_k, θ, and β_k describe the oscillator strength , the phase, and hyperpolarizability of the vibrational mode k, respectively. In eq 3, N describes the molecular number density, while $f(\Omega)$ gives the distribution of $\beta_k(\Omega)$ over the solid angle Ω. Therefore, A_k is linearly dependent on the number density N of adsorbed molecules and the orientational average of the molecules' hyperpolarizability β_k. Because the second-order $\chi^{(2)}$ and third-order $\chi^{(3)}$ contributions are resonantly enhanced when the frequency ω_{IR} is tuned over vibrational modes of interfacial molecules, these equations show how SFG spectroscopy is molecule specific and thus provides qualitative information on the composition[43−46] and the charging state[13,47,48] of proteins at interfaces.

Figure 2 shows the pH-induced changes in the SFG spectra from air−water interfaces that were modified by native and FITC-labeled BSA. In the frequency range from 2800 to 3800 cm^{-1}, the SFG spectra are dominated by two broad bands centered at 3200 and 3450 cm^{-1}. The latter bands arise from O−H stretching modes of tetrahedrally (low frequency modes) and nontetrahedrally (high frequency modes) coordinated interfacial H_2O.[26,27] Because of their dipole character, the interfacial water molecules orientate themselves in accordance with the surface net charge. For pH values below the IEP, the protein molecules carry a positive net charge because of the protonation of the aminogroups and a negative net charge for pH values above the IEP. This is caused by deprotonation of amino acid residues with carboxylate groups. As a consequence, interfacial water molecules flip their orientation by 180°. Similar effects have been observed in phase-resolved SFG measurements of cationic cetyl trimethylammonium bromide and anionic sodium dodecyl sulfate surfactants at the air−water interface reported earlier by the Tahara group.[49] At this point, we recall that the amplitude A_k (eq 3) is an average over all molecular orientations at the interface, and its polarity thus provides information on the net orientation of molecules at interfaces.[48] Therefore, the change in net orientation of interfacial H_2O will result in change of the phase θ by π in eq 2.[13] In this case, evidence for a charge reversal at the interface comes from the polarity of aromatic C−H stretching vibrations at 3060 cm^{-1}. The shape of this band is dominated by the interference of the aromatic C−H stretching with the O−H stretching bands. When the water

DOI: 10.1021/acs.jpcb.8b06481
J. Phys. Chem. B 2018, 122, 10377−10383

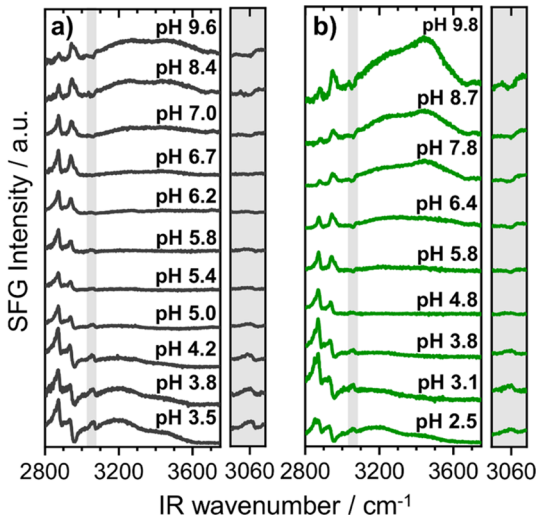

Figure 2. pH dependent changes of SFG spectra from air−water interfaces that were modified by native (a) and FITC-labeled (b) BSA proteins. The frequency region that is presented in the figure is dominated by C−H and O−H stretching vibrations as explained in detail in the main text. The protein concentration in (a) and (b) was fixed to 50 μM. Gray-shaded areas show a close-up of the aromatic C−H stretching band at 3060 cm^{-1}. Note that the shape of this band can be used to determine the net orientation of interfacial H_2O (see main text).

molecules reorientate with the dipole moment pointing away from the bulk, the peak-like feature at ∼3060 cm^{-1} flips into a dip-like feature. This appearance of the aromatic C−H stretching band in the SFG spectra is caused by constructive and destructive interferences with the O−H band.[13] Note that in the Supporting Information, we provide simulations of the latter changes of the shape of the 3060 cm^{-1} band when the phase of the O−H band and thus the molecular orientation of interfacial water molecules are changed accordingly.

In fact, this change can be best seen by a comparison of the SFG spectra for solutions with pH 3 and 10 (Figure 2a, gray-shaded area). The apparent change in polarity of the aromatic C−H stretching band can be, therefore, associated to the polarity of the water bands, which follows the change in net orientation of interfacial H_2O molecules. The latter can be polarized and ordered within the interfacial electric field. Obviously, the apparent change in the polarity of O−H bands is a direct consequence of the charge reversal at the interface. Note that Meister et al.[50] report in their SFG study of hydrophobins at the air−water interface also a pH-induced reorientation of the interfacial proteins which have, in the case of hydrophobins, largely separated hydrophilic and hydrophobic regions. This effect is different in the case of BSA, where the latter are statistically distributed over the protein surface.

The change in SF intensity with pH of both O−H stretching bands as seen Figures 1c and 2, can be qualitatively also explained by changes in the interfacial net charge. Whether the changes in charging with pH at the interface are similar to those in the bulk are hitherto unknown. As $\chi^{(3)}$ contributions to the SF intensity are dependent on the surface potential ϕ_0 (eq 1), we can relate the observed changes in SF intensity directly to variations in the surface potential and thus to the interfacial net charge. Although quantification[40,41] from SFG spectroscopy is difficult, arguments on qualitative changes of the interfacial charging state can be made based on SF intensities (Figures 1b and 2). The minima in O−H intensities which are clearly seen for native and FITC-labeled BSA at pH values close to their bulk IEPs can be therefore directly attributed to a charge reversal at the interface with an interfacial IEP close to the bulk IEP.

The described shift of the IEP, which is seen in both ζ-potential and SFG measurements, is also reflected in the surface tension data plotted in Figure 1b. Here, a local minimum of ∼53 mN m^{-1} is established at pH values close to the bulk and interfacial IEPs of native and labeled BSA proteins. The minimum in surface tension for both BSA proteins is a direct consequence of the loss in net charge at pH values close to the IEP, which reduces the electrostatic repulsive interactions at the interface. Hereby, more protein molecules can place themselves at the surface, what directly increases the surface excess and consequently lower the surface tension. This conclusion is corroborated by previous studies of BSA, BLG, and lysozyme proteins that show a substantial increase in thickness of the adsorbate layers once the electrostatic repulsion forces have been canceled either by choosing a pH close to the IEP or by adding salt.[6,7,13,14,49] The increased surface excess and layer thickness around the IEP could also be directly shown by pH-dependent neutron reflectometry studies.[51] FITC-labeled BSA proteins show substantial bulk aggregation as the solutions become obviously turbid for pH values close to the IEP (between pH ∼3.7 and ∼5.4). Such an obvious turbidity is not observed for native BSA. The differences in bulk behavior of FITC-labeled and native BSA can be explained by the more hydrophobic character of labeled BSA with roughly 12 FITC ligands per BSA molecule (see Experimental Section).

An analysis of the dynamic changes in the surface tension (Supporting Information) reveals a much faster decrease in surface tension at a pH close to the IEP. This observation is consistent with an earlier study by Ulaganathan et al.[22] on the changes in surface tension and the surface dilational modulus of BLG proteins. The observed faster adsorption kinetics, close to the IEP, is typical for proteins in general because of the significantly decreased adsorption barrier caused by reduced electrostatics in this pH range.[52,53] In Figure S4 (Supporting Information), we present results from single foam films using a thin-film pressure balance and demonstrate the existence of aggregates over a broad range of pH values. This may be caused by the close packing of proteins at the interface where much shorter nearest neighbor distances as compared to the situation in the bulk solution are established, but deserves further investigation in the future.

Additional foaming experiments were performed and show that the foam stability reaches a maximum at the IEP (Figure 1d) while the mean bubble size is minimized at the IEP (Figure 3). Particularly, the latter is directly related to the faster adsorption kinetics at the IEP as discussed above. The increased foam stability at the IEP is however, hitherto not fully understood.

In earlier work,[6,7,14] it was hypothesized that the aggregates could block plateau borders and prevent or slowdown foam drainage as this was seen also for other foams stabilized by inorganic and organic particles (see Introduction section). In order to further reveal the location of proteins and protein aggregation inside the foam, we have applied confocal fluorescence microscopy at foams from FITC-labeled BSA solution. These experiments are, in particular, useful to clarify

DOI: 10.1021/acs.jpcb.8b06481
J. Phys. Chem. B 2018, 122, 10377−10383

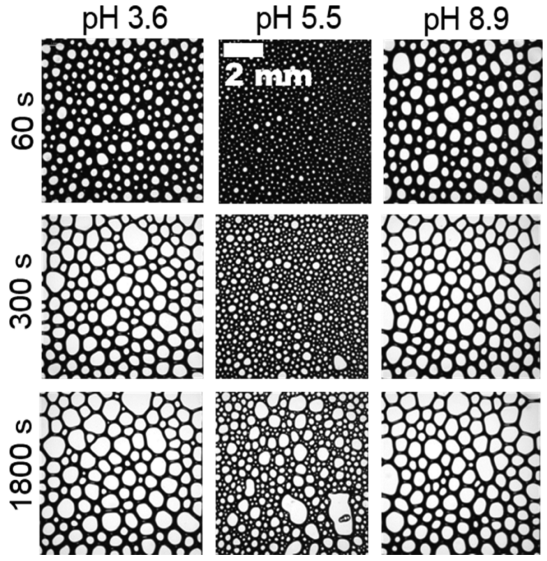

Figure 3. Micrographs of the foam structure for native BSA with a concentration of 50 μM. Time intervals and pH values were as indicated in the figure. Note that the pH of 5.5 is close to the bulk and interfacial IEP at pH 5.3 (main text, Figure 1a). The length scale given in the center column applies for all foam images.

whether an accumulation of protein aggregates in plateau borders or within foam films (lamellae) is relevant for foam stabilization.

In Figure 4, we compare different fluorescence images that were taken along the *z*-axis perpendicular to the focal plane

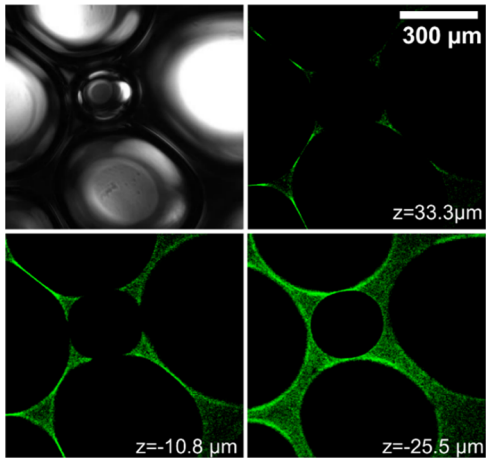

Figure 4. Micrographs from confocal fluorescence microscopy and white light microscopy show images at different arbitrarily chosen *z* positions perpendicular to the imaging plane. The foam/bubbles were formed from a 100 μM BSA-FITC solution at pH 5.7. Signals from FTIC-labeled BSA proteins appear in green color. The scale bar applies for all images.

and compare the latter with a white light image at the same sample position. Regions with green color originate from FITC fluorophores. From a close inspection of Figure 4, sample regions with a higher concentration of fluorescent-labeled BSA can be easily identified by higher fluorescence intensities. From the analysis of Figure 4, we conclude that the presence of proteins and aggregates in the plateau borders does not dominate bubble and foam stabilization because the highest concentrations are in fact observed in the lamellae between bubbles. Consequently, contact zones between bubbles, where two lamellae join, appear with very high fluorescence intensity.

The BSA proteins are distributed all over the lamella. This observation is consistent with our foam film results in Figure S4 (Supporting Information). Note that the presence of aggregates in foam films of BLG solutions has been already shown using the thin-film pressure balance technique.[26] This so far unresolved structure of proteins in foam films may be one origin for the slower foam drainage at pH values close to the IEP as presented in Figure S3 (Supporting Information). In addition, the gas permeability through the foam films could also have changed once the proteins become close-packed inside the foam films—whether this can play an additional role has to await further investigations, for example, with methods proposed earlier by Saulnier et al.[54]

CONCLUSIONS

Using a multitechnique approach, we address the stabilization of aqueous foam from BSA solutions on several length scales and derive structure−property relations. Vibrational SFG spectroscopy and ζ-potential measurements are used to study the charging state of native and FITC-labeled BSA molecules at the air−water interface and in the bulk solution. The interfacial and the bulk IEPs are found at pH 5.3 and 4.7 for native and labeled BSA, respectively, and are shown to be very similar for proteins in the bulk and at the air−water interface. Our conclusion of closer protein packing at pH values close to the IEP is corroborated by our surface tension and previous thickness measurements of BSA adsorbate layers. Different from the classical DLVO theory, which would predict a decrease in electrostatic disjoining pressure and thus foam stability, we confirm that negligible electrostatic interactions between BSA molecules at the interface lead to a pronounced increase in foam stability.

Using confocal fluorescence microscopy of foams from solution with FITC-labeled BSA, we clarified that BSA molecules are predominantly located in the foam films (lamellae) which connect individual bubbles. Our study shows that BSA molecules lead to a different mechanism for foam stabilization in comparison to previously discussed nanoparticle-stabilized foams, where the particles blocked plateau borders.

Besides a stronger aggregation near the IEP due to a higher hydrophobicity, the FITC-labeled BSA showed the same characteristic surface behavior. For that reason, we propose that the results of our study may be transferrable to other but similar proteins like BLG.

ASSOCIATED CONTENT

Supporting Information

The Supporting Information is available free of charge on the ACS Publications website at DOI: 10.1021/acs.jpcb.8b06481.

Description of the broadband SFG set-up, molecular structure of the FITC-labeled BSA, dynamic surface tension for BSA adsorption to the air−water interface from solutions with different bulk pH, foam drainage and pH dependence of the liquid fraction inside foam, and thin-film pressure balance measurements for 50 μm BSA foam films at pH values above/below and at the IEP (PDF)

DOI: 10.1021/acs.jpcb.8b06481
J. Phys. Chem. B 2018, 122, 10377−10383

AUTHOR INFORMATION

Corresponding Author

*E-mail: braunschweig@uni-muenster.de.

ORCID

Natalia García Rey: 0000-0002-9175-3416

Björn Braunschweig: 0000-0002-6539-1693

Notes

The authors declare no competing financial interest.

ACKNOWLEDGMENTS

The authors are grateful for the support of Professor Dr. Ing. Wolfgang Peukert (FAU Erlangen-Nürnberg) and for allowing us to use the confocal microscope at the Institute of Particle Technology (LFG). We also thank Helena Rippel for experimental assistance and Dr. Georgi Gochev for helpful discussions. Furthermore, we are thankful for the funding of the European Research Council (ERC) under the European Union's Horizon 2020 research and innovation program (grant agreement no. 638278) and Deutsche Forschungsgemeinschaft (DFG).

REFERENCES

(1) Koepf, E.; Richert, M.; Braunschweig, B.; Schroeder, R.; Brezesinski, G.; Friess, W. Impact of Formulation pH on Physicochemical Protein Characteristics at the Liquid-Air Interface. *Int. J. Pharm.* **2018**, *541*, 234−245.

(2) Kannan, A.; Shieh, I. C.; Leiske, D. L.; Fuller, G. G. Monoclonal Antibody Interfaces: Dilatation Mechanics and Bubble Coalescence. *Langmuir* **2018**, *34*, 630−638.

(3) Winner, B.; Jappelli, R.; Maji, S. K.; Desplats, P. A.; Boyer, L.; Aigner, S.; Hetzer, C.; Loher, T.; Vilar, M.; Campioni, S.; et al. In vivo demonstration that -synuclein oligomers are toxic. *Proc. Natl. Acad. Sci. U.S.A.* **2011**, *108*, 4194−4199.

(4) Ahmedna, M.; Prinyawiwatkul, W.; Rao, R. M. Solubilized Wheat Protein Isolate: Functional Properties and Potential Food Applications†. *J. Agric. Food Chem.* **1999**, *47*, 1340−1345.

(5) Wierenga, P. A.; Gruppen, H. New Views on Foams From Protein Solutions. *Curr. Opin. Colloid Interface Sci.* **2010**, *15*, 365−373.

(6) Engelhardt, K.; Lexis, M.; Gochev, G.; Konnerth, C.; Miller, R.; Willenbacher, N.; Peukert, W.; Braunschweig, B. pH Effects on the Molecular Structure of β-Lactoglobulin Modified Air-Water Interfaces and Its Impact on Foam Rheology. *Langmuir* **2013**, *29*, 11646−11655.

(7) Engelhardt, K.; Rumpel, A.; Walter, J.; Dombrowski, J.; Kulozik, U.; Braunschweig, B.; Peukert, W. Protein Adsorption at the Electrified Air-Water Interface: Implications on Foam Stability. *Langmuir* **2012**, *28*, 7780−7787.

(8) Rullier, B.; Novales, B.; Axelos, M. A. V. Effect of protein aggregates on foaming properties of β-lactoglobulin. *Colloids Surf., A* **2008**, *330*, 96−102.

(9) Rullier, B.; Axelos, M. A. V.; Langevin, D.; Novales, B. β-Lactoglobulin aggregates in foam films: Correlation between foam films and foaming properties. *J. Colloid Interface Sci.* **2009**, *336*, 750−755.

(10) Campbell, R. A.; Tummino, A.; Varga, I.; Milyaeva, O. Y.; Krycki, M. M.; Lin, S.-Y.; Laux, V.; Haertlein, M.; Forsyth, V. T.; Noskov, B. A. Adsorption of Denaturated Lysozyme at the Air-Water Interface: Structure and Morphology. *Langmuir* **2018**, *34*, 5020−5029.

(11) Beierlein, F. R.; Clark, T.; Braunschweig, B.; Engelhardt, K.; Glas, L.; Peukert, W. Carboxylate Ion Pairing with Alkali-Metal Ions for β-Lactoglobulin and Its Role on Aggregation and Interfacial Adsorption. *J. Phys. Chem. B* **2015**, *119*, 5505−5517.

(12) Engelhardt, K.; Weichsel, U.; Kraft, E.; Segets, D.; Peukert, W.; Braunschweig, B. Mixed Layers of β-Lactoglobulin and SDS at Air-Water Interfaces with Tunable Intermolecular Interactions. *J. Phys. Chem. B* **2014**, *118*, 4098−4105.

(13) Engelhardt, K.; Peukert, W.; Braunschweig, B. Vibrational sum-frequency generation at protein modified air-water interfaces: Effects of molecular structure and surface charging. *Curr. Opin. Colloid Interface Sci.* **2014**, *19*, 207−215.

(14) Braunschweig, B.; Schulze-Zachau, F.; Nagel, E.; Engelhardt, K.; Stoyanov, S.; Gochev, G.; Khristov, K.; Mileva, E.; Exerowa, D.; Miller, R.; et al. Specific effects of Ca^{2+} ions and molecular structure of β-lactoglobulin interfacial layers that drive macroscopic foam stability. *Soft Matter* **2016**, *12*, 5995−6004.

(15) Dimitrova, L. M.; Petkov, P. V.; Kralchevsky, P. A.; Stoyanov, S. D.; Pelan, E. G. Production and Characterization of Stable Foams with Fine Bubbles from Solutions of Hydrophobin HFBII and its Mixtures With Other Proteins. *Colloids Surf., A* **2017**, *521*, 92−104.

(16) Chen, M.; Feijen, S.; Sala, G.; Meinders, M. B. J.; van Valenberg, H. J. F.; van Hooijdonk, A. C. M.; van der Linden, E. Foam Stabilized By Large Casein Micelle Aggregates: The Effect of Aggregate Number in Foam Lamella. *Food Hydrocolloids* **2018**, *74*, 342−348.

(17) Mahler, H.-C.; Friess, W.; Grauschopf, U.; Kiese, S. Protein Aggregation: Pathways, Induction Factors and Analysis. *J. Pharm. Sci.* **2009**, *98*, 2909−2934.

(18) Rathore, N.; Rajan, R. S. Current Perspectives on Stability of Protein Drug Products during Formulation, Fill and Finish Operations. *Biotechnol. Prog.* **2008**, *24*, 504−514.

(19) Löwik, D. W. P. M.; van Hest, J. C. M. Peptide based amphiphiles. *Chem. Soc. Rev.* **2004**, *33*, 234−245.

(20) Petkova, V.; Sultanem, C.; Nedyalkov, M.; Benattar, J.-J.; Leser, M. E.; Schmitt, C. Structure of a Freestanding Film of β-Lactoglobulin. *Langmuir* **2003**, *19*, 6942−6949.

(21) Cascão Pereira, L. G.; Johansson, C.; Radke, C. J.; Blanch, H. W. Surface Forces and Drainage Kinetics of Protein-Stabilized Aqueous Films. *Langmuir* **2003**, *19*, 7503−7513.

(22) Ulaganathan, V.; Retzlaff, I.; Won, J. Y.; Gochev, G.; Gunes, D. Z.; Gehin-Delval, C.; Leser, M.; Noskov, B. A.; Miller, R. β-Lactoglobulin adsorption layers at the water/air surface: 2. Dilational rheology: Effect of pH and ionic strength. *Colloids Surf., A* **2017**, *521*, 167−176.

(23) Bergeron, V. Forces and Structure in Thin Liquid Soap Films. *J. Phys.: Condens. Matter* **1999**, *11*, R215−R238.

(24) Stubenrauch, C.; von Klitzing, R. Disjoining Pressure in Thin Liquid Foam and Emulsion Films - New Concepts and Perspectives. *J. Phys.: Condens. Matter* **2003**, *15*, R1197−R1232.

(25) Israelachvilli, J. N. *Intermolecular and Surface Forces*, 3rd ed.; Academic Press, 2011.

(26) Gochev, G.; Retzlaff, I.; Exerowa, D.; Miller, R. Electrostatic stabilization of foam films from β-lactoglobulin solutions. *Colloids Surf., A* **2014**, *460*, 272−279.

(27) Zawala, J.; Todorov, R.; Olszewska, A.; Exerowa, D.; Malysa, K. Influence of pH of the BSA solutions on velocity of the rising bubbles and stability of the thin liquid films and foams. *Adsorption* **2010**, *16*, 423−435.

(28) Lexis, M.; Willenbacher, N. Relating foam and interfacial rheological properties of β-lactoglobulin solutions. *Soft Matter* **2014**, *10*, 9626−9636.

(29) Zhang, L.; Tian, L.; Du, H.; Rouzière, S.; Wang, N.; Salonen, A. Foams Stabilized by Surfactant Precipitates: Criteria for Ultrastability. *Langmuir* **2017**, *33*, 7305−7311.

(30) Carl, A.; Bannuscher, A.; von Klitzing, R. Particle Stabilized Aqueous Foams at Different Length Scales: Synergy between Silica Particles and Alkylamines. *Langmuir* **2015**, *31*, 1615−1622.

(31) Fameau, A.-L.; Saint-Jalmes, A.; Cousin, F.; Houinsou Houssou, B.; Novales, B.; Navailles, L.; Nallet, F.; Gaillard, C.; Boué, F.; Douliez, J.-P. Smart Foams: Switching Reversibly between Ultrastable and Unstable Foams. *Angew. Chem.* **2011**, *50*, 8264−8269.

(32) Lazidis, A.; Hancocks, R. D.; Spyropoulos, F.; Kreuß, M.; Berrocal, R.; Norton, I. T. Whey Protein Fluid Gels for the Stabilisation of Foams. *Food Hydrocolloids* **2016**, *53*, 209−217.

DOI: 10.1021/acs.jpcb.8b06481
J. Phys. Chem. B 2018, 122, 10377−10383

(33) Schmitt, C.; Bovay, C.; Rouvet, M. Bulk self-aggregation drives foam stabilization properties of whey protein microgels. *Food Hydrocolloids* **2014**, *42*, 139−148.
(34) Kolodziejczyk, E.; Petkova, V.; Benattar, J.-J.; Leser, M. E.; Michel, M. Effect of fluorescent labeling of β-lactoglobulin on film and interfacial properties in relation to confocal fluorescence microscopy. *Colloids Surf., A* **2006**, *279*, 159−166.
(35) Khalfan, H.; Abuknesha, R.; Rand-Weaver, M.; Price, R. G.; Robinson, D. Aminomethyl Coumarin Acetic Acid: A New Fluorescent Labelling Agent for Proteins. *Histochem. J.* **1986**, *18*, 497−499.
(36) Richards, D. P.; Stathakis, C.; Polakowski, R.; Ahmadzadeh, H.; Dovichi, N. J. Labeling Effects on the Isoelectric Point of Green Fluorescent Protein. *J. Chromatogr. A* **1999**, *853*, 21−25.
(37) Gonella, G.; Lütgebaucks, C.; de Beer, A. G. F.; Roke, S. Second Harmonic and Sum-Frequency Generation from Aqueous Interfaces Is Modulated by Interference. *J. Phys. Chem. C* **2016**, *120*, 9165−9173.
(38) Schaefer, J.; Gonella, G.; Bonn, M.; Backus, E. H. G. Surface-Specific Vibrational Spectroscopy of the Water/Silica Interface: Screening and Interference. *Phys. Chem. Chem. Phys.* **2017**, *19*, 16875−16880.
(39) Ohno, P. E.; Saslow, S. A.; Wang, H.-f.; Geiger, F. M.; Eisenthal, K. B. Phase-referenced nonlinear spectroscopy of the α-quartz/water interface. *Nat. Commun.* **2016**, *7*, 13587.
(40) Ohno, P. E.; Wang, H.-f.; Geiger, F. M. Second-Order Spectral Lineshapes From Charged Interfaces. *Nat. Commun.* **2017**, *8*, 1032.
(41) Ohno, P. E.; Wang, H.-f.; Paesani, F.; Skinner, J. L.; Geiger, F. M. Second-Order Vibrational Lineshapes from the Air/Water Interface. *J. Phys. Chem. A* **2018**, *122*, 4457−4464.
(42) Morita, A. *Theory of Sum Frequency Generation Spectroscopy: Lecture Notes in Chemistry*; Springer: Singapore, 2018.
(43) Meister, K.; Paananen, A.; Speet, B.; Lienemann, M.; Bakker, H. J. Molecular Structure of Hydrophobins Studied with Site-Directed Mutagenesis and Vibrational Sum-Frequency Generation Spectroscopy. *J. Phys. Chem. B* **2017**, *121*, 9398−9402.
(44) Weidner, T.; Breen, N. F.; Drobny, G. P.; Castner, D. G. Amide or Amine: Determining the Origin of the 3300 cm^{-1} NH Mode in Protein SFG Spectra Using15N Isotope Labels. *J. Phys. Chem. B* **2009**, *113*, 15423−15426.
(45) Xiao, M.; Jasensky, J.; Foster, L.; Kuroda, K.; Chen, Z. Monitoring Antimicrobial Mechanisms of Surface-Immobilized Peptides in Situ. *Langmuir* **2018**, *34*, 2057−2062.
(46) Hall, S. A.; Jena, K. C.; Covert, P. A.; Roy, S.; Trudeau, T. G.; Hore, D. K. Molecular-Level Surface Structure from Nonlinear Vibrational Spectroscopy Combined with Simulations. *J. Phys. Chem. B* **2014**, *118*, 5617−5636.
(47) Dreier, L. B.; Nagata, Y.; Lutz, H.; Gonella, G.; Hunger, J.; Backus, E. H. G.; Bonn, M. Saturation of Charge-Induced Water Alignment at Model Membrane Surfaces. *Sci. Adv.* **2018**, *4*, eaap7415.
(48) Shen, Y. R.; Ostroverkhov, V. Sum-Frequency Vibrational Spectroscopy on Water Interfaces: Polar Orientation of Water Molecules at Interfaces. *Chem. Rev.* **2006**, *106*, 1140−1154.
(49) Nihonyanagi, S.; Mondal, J. A.; Yamaguchi, S.; Tahara, T. Structure and Dynamics of Interfacial Water Studied by Heterodyne-Detected Vibrational Sum-Frequency Generation. *Annu. Rev. Phys. Chem.* **2013**, *64*, 579−603.
(50) Meister, K.; Roeters, S. J.; Paananen, A.; Woutersen, S.; Versluis, J.; Szilvay, G. R.; Bakker, H. J. Observation of pH-Induced Protein Reorientation at the Water Surface. *J. Phys. Chem. Lett.* **2017**, *8*, 1772−1776.
(51) Lu, J. R.; Su, T. J.; Penfold, J. Adsorption of Serum Albumins at the Air/Water Interface. *Langmuir* **1999**, *15*, 6975−6983.
(52) Ulaganathan, V.; Retzlaff, I.; Won, J. Y.; Gochev, G.; Gehin-Delval, C.; Leser, M.; Noskov, B. A.; Miller, R. β-Lactoglobulin adsorption layers at the water/air surface: 1. Adsorption kinetics and surface pressure isotherm: Effect of pH and ionic strength. *Colloids Surf., A* **2017**, *519*, 153−160.
(53) Duchin, S. S.; Kretzschmar, G.; Miller, R. *Dynamics of Adsorption at Liquid Interfaces: Theory, Experiment, Application*; Elsevier: Amsterdam, 1995.
(54) Saulnier, L.; Drenckhan, W.; Larré, P.-E.; Anglade, C.; Langevin, D.; Janiaud, E.; Rio, E. In Situ Measurement of the Permeability of Foam Films Using Quasi-Two-Dimensional Foams. *Colloids Surf., A* **2015**, *473*, 32−39.

DOI: 10.1021/acs.jpcb.8b06481
J. Phys. Chem. B 2018, 122, 10377−10383